Applied Catalysis B: Environmental 325 (2023) 122329

Contents lists available at ScienceDirect

Applied Catalysis B: Environmental

journal homepage: www.elsevier.com/locate/apcatb

Catalytic direct dehydrogenation of ethyl lactate to produce ethyl pyruvate over a synergetic Cu^0/Cu^+ interface

Shiyao Lu [a], Jian Zhang [a,*], Hao Meng [a], Xiaoyuan Qin [a], Jianbin Huang [a], Yehao Liang [a], Feng-Shou Xiao [a,b,**]

[a] Beijing Advanced Innovation Center for Soft Matter, Science and Engineering, Beijing University of Chemical Technology, Beijing, China
[b] Key Lab of Biomass Chemical Engineering of Ministry of Education, College of Chemical and Biological Engineering, Zhejiang University, Hangzhou 310027, China

ARTICLE INFO

Keywords:
Biomass conversion
Ethyl lactate
Ethyl pyruvate
Cu catalyst
Synergism

ABSTRACT

The direct dehydrogenation of ethyl lactate (EL) to produce ethyl pyruvate (EP) over non-precious heterogeneous catalysts is highly desirable, but challenging. Herein, we report a highly efficient silica-supported copper catalyst prepared *via* a hydrolysis-precipitation method (Cu/SiO_2-HP) for the dehydrogenation of ethyl lactate, which exhibited an 85.4 % EL conversion with 91.1 % selectivity toward EP at 320 °C. XAFS, *in situ* XPS, and CO-adsorption FT-IR spectra revealed that the Cu/SiO_2-HP catalyst had abundant Cu^0/Cu^+ interfaces. *In situ* FT-IR spectra, kinetic studies, and theoretical calculations also demonstrated that the Cu^0/Cu^+ interfaces synergistically activate the O–H and C–H bonds in the adsorbed EL for direct dehydrogenation into EP. The H/D kinetic isotope effect for model reaction confirmed that C–H bond activation is the key step in the dehydrogenation reaction. This study offers a new approach toward the selective conversion of EL into EP, which is of great significance for biomass conversion.

1. Introduction

The catalytic conversion of biomass platform molecules into valuable products has received considerable attentions due to the increasing demand for sustainable development [1–4]. For example, ethyl lactate (EL) is an important platform molecule that can be produced *via* the conversion of cellulose, starch, and other sugars [5–15]. EL can be converted into ethyl pyruvate (EP) *via* heterogeneous catalysis, which has been applied in the synthesis of various pharmaceuticals and dietary supplements [5–15]. Typically, EL is converted by catalytic oxidation reactions [1–15], which provided opportunities for the investigation of mechanisms in the production of carbonyls [16–20]. Mixed metal oxide catalysts, such as mesoporous vanadium oxide–titanium oxide, transition metal phosphate nanolayers, and iron antimonates, are employed using O_2 or air as the oxidant [2,5,6,10,14,15]. However, EP is unstable when exposed to O_2, forming by-products due to over-oxidation. Consequently, the selectivity toward EP during EL oxidation is normally less than 90 % [2,5,6,10,14,15]. Therefore, the catalytic conversion of EL to EP under O_2-free conditions is significantly desirable.

It is well known that alcohols can be converted to their corresponding aldehydes (or ketones) *via* direct dehydrogenation [21–26], which effectively diminishes the side-products by over-oxidations. For example, Cu-containing catalysts are efficient for the dehydrogenation of ethanol into acetaldehyde, giving very high selectivity for acetaldehyde [23]. Considering the similarity between the dehydrogenation of ethanol to acetaldehyde and the dehydrogenation of EL to EP, it is reasonable to expect the achievement of high EP selectivity in the direct dehydrogenation of EL. However, the direct dehydrogenation of EL to produce EP using heterogeneous catalysis has rarely been reported to date, and the development of efficient catalysts as well as a systematic investigation of the reaction mechanism are challenging, but extremely valuable.

Herein, we report the preparation of supported Cu nanoparticles from hydrolysis–precipitation method, which are highly efficient for the selective dehydrogenation of EL to produce EP, giving an EL conversion of 85.4 % with EP selectivity of 91.1 % at 320 °C. Characterizations, kinetic studies, and calculation results have confirmed that the synergism between Cu^+ and Cu^0 in the Cu/SiO_2-HP catalyst is crucial for the

* Corresponding author.
** Corresponding author at: Beijing Advanced Innovation Center for Soft Matter, Science and Engineering, Beijing University of Chemical Technology, Beijing, China.
E-mail addresses: jianzhangbuct@mail.buct.edu.cn (J. Zhang), fsxiao@zju.edu.cn (F.-S. Xiao).

https://doi.org/10.1016/j.apcatb.2022.122329
Received 22 August 2022; Received in revised form 19 December 2022; Accepted 26 December 2022
Available online 31 December 2022

excellent catalytic results, which activate the O−H and C−H bonds in the adsorbed EL molecules, respectively. The construction of abundant Cu^0/Cu^+ interfaces is significant for the development of an efficient catalyst for the dehydrogenation of EL to produce EP.

2. Experimental section

2.1. Materials

Ethanol, alumina (γ-Al_2O_3, AR), magnesium oxide (MgO, AR), ammonia (25–28 *wt.*%), ammonium carbonate ($(NH_4)_2CO_3$, AR) were purchased from Sino-Pharm Chemical Reagent Co., Ltd. Anatase (TiO_2, AR) were bought from Alfa Aesar Chemical Co., Ltd. Tetraethylorthosilicate (TEOS, AR) were bought from Aladdin Chemical Co., Ltd. Copper nitrate trihydrate ($Cu(NO_3)_2{\cdot}3\ H_2O$, AR) was purchased from Macklin Chemical Co., Ltd. LUDOX AS-30 colloidal silica (30 *wt.*%) was purchased from Sigma-Aldrich Co., Ltd. Copper (I) oxide (Cu_2O, AR) and copper (II) oxide (CuO, AR) were purchased from Adamas Chemical Reagent Co., Ltd. Deuterium-substituted ethanols [1-D-ethanol (99 atom %D) and ethanol-d_6 (99 atom%D)] were purchased from J&K Chemical Co., Ltd.

2.2. Synthesis of Cu/SiO_2-HP

The synthesis of Cu/SiO_2-HP was from hydrolysis-precipitation (HP) method with a little modification, reported previously [27]. Typically, 3.207 g of $Cu(NO_3)_2{\cdot}3\ H_2O$ was added into a mixed solution of 12.790 g of TEOS, 20.000 mL of ethanol, and 13.000 g of H_2O, stirring for 1 h, which was designated as mixture A. Meanwhile, 3.063 g of $(NH_4)_2CO_3$ was dissolved into 127.000 g of H_2O, which was designated as mixture B. Then, mixture A and mixture B were simultaneously added into 100.000 g of H_2O at 80 °C under vigorous stirring, and the pH value of the obtained mixture was kept at ~7. After the precipitation, the obtained mixture was kept stirring for another 18 h at 80 °C. After filtrating, washing with a large amount of H_2O, drying at 80 °C overnight, and calcining at 400 °C for 4 h in static air, the Cu/SiO_2-HP was finally obtained. The Cu loading could be adjusted by changing the amount of $Cu(NO_3)_2{\cdot}3\ H_2O$ added in the starting mixture A (Table S1). If not mentioned, the Cu/SiO_2-HP was the sample with Cu loading at 15.1 *wt* %.

2.3. Characterizations

X-ray diffraction (XRD) patterns were measured on a Bruker AXS D8 FOCUS diffractometer with Cu Kα radiation (λ = 1.5418 Å). Nitrogen-sorption isotherms were measured using a MicrotracBEL MINI II 2460 physisorption instrument. The samples were vacuum treated at 120 °C overnight before tests. Cu loadings were determined by inductively coupled plasma (ICP) analysis (Perkin-Elmer 3300DV). The Cu-containing samples were dissolved by a mixture solution of HF and nitric acid, followed by dilution to a certain volume for the tests. High resolution transmission electron microscopy (HR-TEM), scanning transmission electron microscopy (STEM), and elemental mapping were obtained on a JEOL JEM-3100 F electron microscope with an acceleration voltage of 300 kV. Temperature-programmed desorption of H_2 and EP (H_2-TPD and EP-TPD) were performed on a BELCAT-B chemisorption instrument equipped with a thermal conductivity detector (TCD). The samples were firstly pretreated at 300 °C in flowing H_2 (30 mL/min) for 1 h and subsequently adsorbed the adsorbates (H_2 or EP) at 50 °C. After sweeping the samples at 50 °C for 1 h with flowing He (30 mL/min) to remove the physisorbed adsorbates, the samples were heated with a rate of 10 °C/min to desorb the chemisorbed adsorbates.

Cu dispersion (D_{Cu}) of the Cu catalysts were detected by N_2O titration on a Huasi DAS-T200 chemisorption instrument. The catalyst was pre-reduced at 300 °C for 1 h in flowing H_2 (30 mL/min) (Fig. S1). Then, the catalyst was cooled to 50 °C and treated with 10 % N_2O/Ar (30 mL/min) to selectively oxidize the surface Cu atoms to + 1 valence state. Afterwards, the catalyst was temperature-programmed reduced in following H_2/N_2 (30 mL/min) with a ramp rate of 10 °C/min to 500 °C. The consumed H_2 amount was designated as H_T. Then, the catalyst was thoroughly re-oxidized in flowing pure O_2 (30 mL/min) at 300 °C for 1 h. The re-oxidized catalysts were temperature-programmed reduced again in following H_2/N_2 (30 mL/min) with a ramp rate of 10 °C/min to 700 °C. The consumed H_2 amount was designated as H_0. The Cu dispersion was calculated with equation in the following:

$$D_{Cu} = \frac{2 \cdot H_T}{H_0} \tag{1}$$

The copper specific surface area (S_{Cu}) was calculated using equation in the following:

$$S_{Cu} = \frac{2 \cdot H_T \cdot N_A}{H_0 \cdot M_{Cu} \cdot SD_{Cu}} \left(m^2/g_{Cu}\right) \tag{2}$$

where N_A is Avogadro's number (6.022×10^{23} /mol), M_{Cu} is atomic weight of copper (63.546 g/mol), and SD_{Cu} is copper surface density (1.46×10^{19} atoms/m^2).

Furthermore, effective copper diameter (d_{eff}) was estimated using equation with the assumption that the Cu nanoparticles was of hemispherical shape (the surface area of hemisphere is $\pi{\cdot}d_{eff}^2/2$ and the volume of hemisphere is $\pi{\cdot}d_{eff}^3/12$, Fig. S2) in the following:

$$d_{eff} = \frac{6 \cdot \text{volume of hemisphere}}{\text{surface area of hemisphere}} \tag{3}$$

After simplification,

$$d_{eff} = \frac{6}{S_{Cu} \cdot \rho_{Cu}} \left(10^3 \text{nm}\right) \tag{4}$$

where ρ_{Cu} is the density of copper (8.94 g/cm^3). Cu^0-Cu^+ interface perimeter length (L_{int}) was estimated using equation in the following:

$$L_{int} = \frac{2 \cdot S_{Cu}}{d_{eff}} \left(10^6 m/g_{Cu}\right) \tag{5}$$

An example of calculation of the Cu^0-Cu^+ interface length was shown in Table S1.

2.4. Catalytic dehydrogenation of EL to produce EP

Catalytic dehydrogenation of EL to EP was performed on a fixed bed reactor with an inner diameter of 10 mm. The catalysts were pressured, crushed, sieved into 40–60 mesh, and diluted with quartz in the volume ratio of 1/1. The catalysts were pre-reduced at 300 °C for 1 h in H_2 before tests (30 mL/min). The reaction was performed with reactant gas component of 1.20 kPa EL with 100.13 kPa N_2 and GHSV at 16,500 $mL{\cdot}g_{cat}^{-1}{\cdot}h^{-1}$. EL was introduced by a pump (0.2 mL/h) and evaporated before connecting with the catalysts. The gaseous EL was diluted with flowing N_2 (54.3 mL/min), and N_2 flow rate was controlled by a mass flow controller. The productive gas was passed through a cold trap to separate the liquid and gas products. The liquid products (EP and other by-products) and unreacted EL were analyzed by a gas chromatography equipped a HP-5 column (30 m × 0.25 mm × 0.25 μm) and a flame ionized detector (GC-FID) using an internal standard method (ethylbenzene was applied as the internal standard). The EL conversion, EP selectivity, and carbon balance were calculated based on the equations in the following:

$$\text{EL } \textit{conversion} = \frac{V_{\text{EL inlet flow rate}} - V_{\text{EL outlet flow rate}}}{V_{\text{EL inlet flow rate}}} \times 100\%, \tag{6}$$

$$\text{EP } \textit{yield} = \frac{n_{EP} \times V_{\text{EP outlet flow rate}}}{n_{EL} \times V_{\text{EL inlet flow rate}}} \times 100\%, \tag{7}$$

$$\text{EP } \textit{selectivity} = \frac{n_{EP} \times V_{EP\ \text{outlet flow rate}}}{n_{EL} \times (V_{EL\ \text{inlet flow rate}} - V_{EL\ \text{outlet flow rate}})} \times 100\%, \quad (8)$$

$$\text{Other product yield} = \frac{n_i \times V_{i\ \text{outlet flow rate}}}{n_{EL} \times V_{EL\ \text{inlet flow rate}}} \times 100\%, \quad (9)$$

$$\text{Other product } \textit{selectivity} = \frac{n_i \times V_{i\ \text{outlet flow rate}}}{n_{EL} \times (V_{EL\ \text{inlet flow rate}} - V_{EL\ \text{outlet flow rate}})} \times 100\%, \quad (10)$$

$$\text{Carbon mass } \textit{balance} = \frac{\Sigma\, n_i \times V_i}{n_{EL} \times V_{EL\ \text{inlet flow rate}}} \times 100\%, \quad (11)$$

where i stands for EL or the products (including EP, ethanol, and acetaldehyde), n_i stands for the carbon number in EL or the product molecules, and V_i stands for the molar flow rate of EL or the products. During the reaction, the detected side products were acetaldehyde and ethanol, which were resulted from decarboxylation and/or decarbonylation of the ethyl lactate and ethyl pyruvate molecules [28,29]. Furthermore, oligomers and cokes can be also detected on the used catalyst by thermogravimetric analysis-differential scanning calorimetry (TG-DSC) and Fourier transform infrared spectrometer (FT-IR) characterizations.

2.5. Recyclable tests

The recyclable tests were performed on the same reactor for the conversion of EL to EP at 275 °C with WHSV at 0.5 $g_{EL} \cdot g_{cat}^{-1} \cdot h^{-1}$. After dehydrogenation of EL for 23 h, the catalyst was calcined in flowing air (50 mL/min) at 400 °C for 1 h to remove the oligomers/coke, reduced in flowing H_2 (30 mL/min) at 300 °C for 1 h, and cooled to 275 °C in N_2 for the next run.

3. Results and discussion

3.1. Catalyst characterization and dehydrogenation of EL to produce EP

Fig. 1 shows the TEM images and EDS elemental mappings of Cu/SiO_2-HP. Fig. 1a clearly shows that Cu nanoparticles with mean size at ~2.5 nm were highly dispersed on the amorphous SiO_2 support. The Cu nanoparticles exhibited lattice spacings at 0.208 nm [Cu(111) lattice] and 0.180 nm [Cu(200) lattice] on the HR-TEM image (Fig. 1b), which was in accordance with the XRD pattern. As shown in Fig. S3, the Cu/SiO_2-HP sample exhibited peaks at 36.5°, 43.3°, and 50.4° in the XRD pattern. The first peak was associated with the Cu_2O(111) (JCPDS #65–3288) and the remaining peaks were associated with the Cu(111) and Cu(200) lattices of metallic Cu (JCPDS #04–0836). These results confirm the presence of both Cu^0 and Cu^+ species in the Cu/SiO_2-HP sample. STEM and elemental mapping of the Cu, O, and Si species were performed to confirm the high dispersion of the Cu species. As shown in Fig. 1c-f, it was found that the Cu species were surrounded by Si and O species, which was well consistent with that of the TEM image (Fig. 1a). Nitrogen-sorption isotherms were obtained to study the structural parameters of Cu/SiO_2-HP. Two steps were clearly observed in the P/P_0 range of 0.1–0.7 and 0.8–1.0 on the nitrogen-sorption isotherms obtained for Cu/SiO_2-HP (Fig. S4), indicating the presence of hierarchical mesopores. Correspondingly, the surface area and pore volume were 275.4 m^2/g and 0.60 cm^3/g, respectively (Table S1).

The Cu/SiO_2 catalysts were applied for the direct dehydrogenation of EL to produce EP. Fig. 2a shows the dependence of EL conversion and EP yield on the reaction temperature over Cu/SiO_2-HP. Notably, the EL conversion increased upon increasing the reaction temperature, exhibiting ~50.0 % and ~90.0 % conversion at 260 and 330 °C, respectively. However, EP yield varied with the reaction temperature. The EP yield

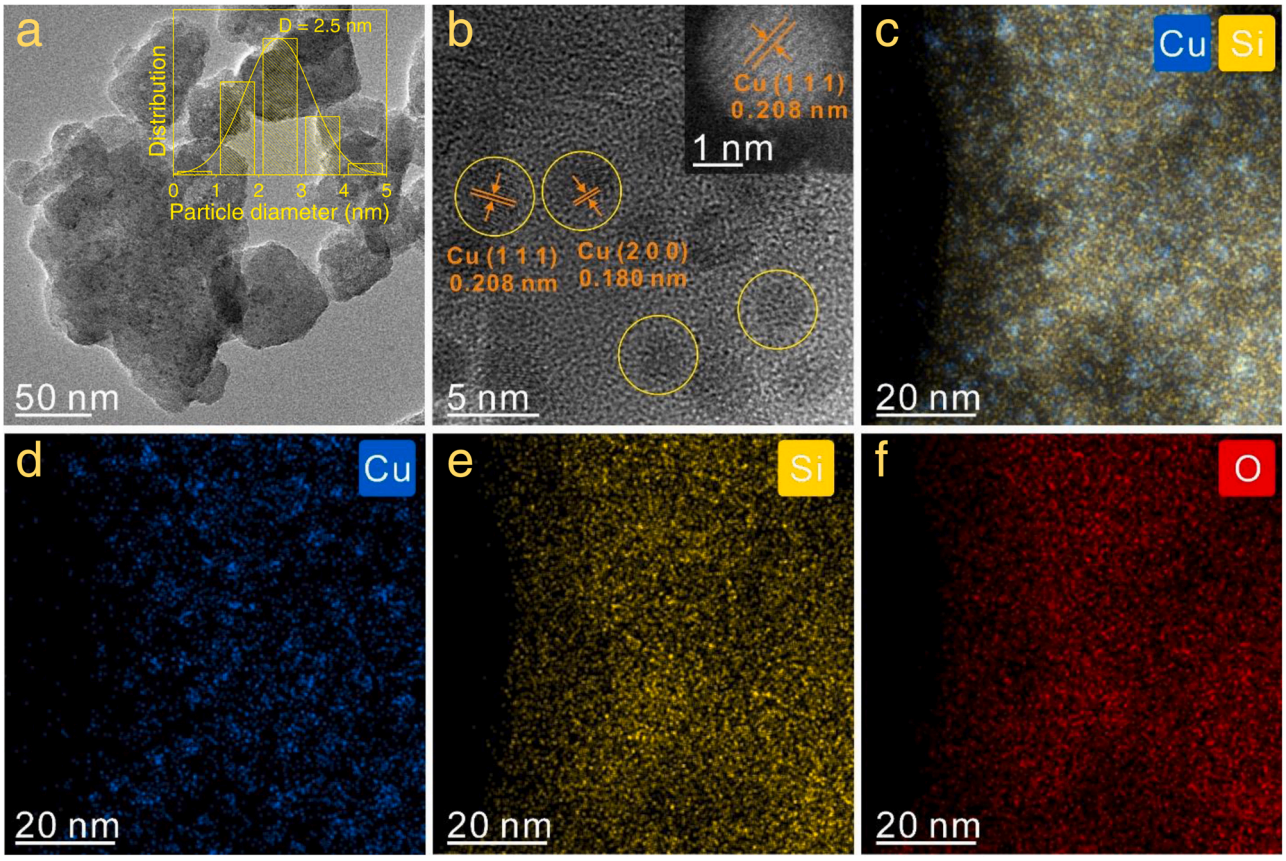

Fig. 1. (a) TEM image, (b) HR-TEM image, and (c–f) EDS elemental mapping of Cu, Si, and O of the Cu/SiO_2-HP sample. Inset in a: Cu nanoparticle size distribution. Inset in b: Enlarged view of a Cu nanoparticle. The yellow circles in b highlighted the Cu nanoparticles in Cu/SiO_2-HP.

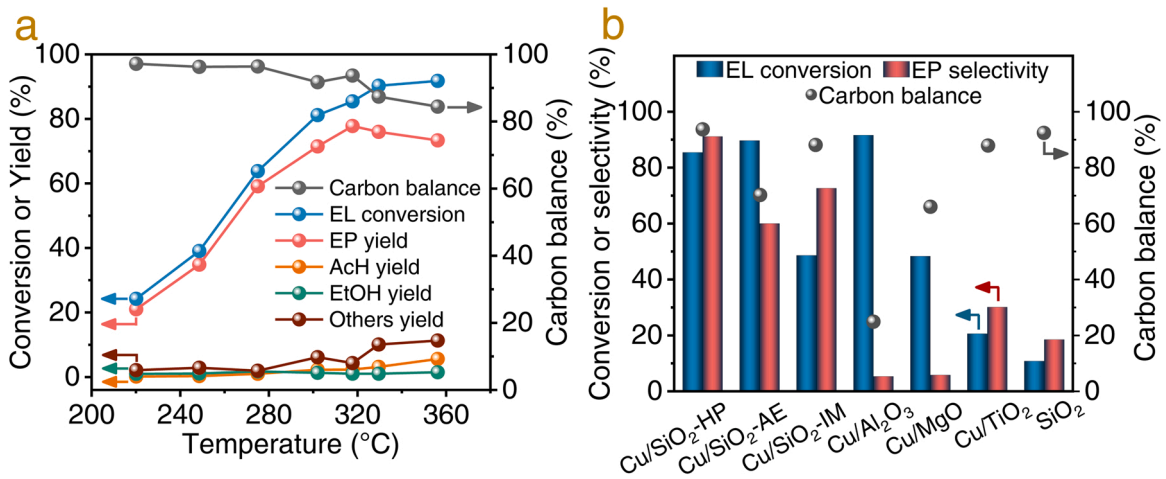

Fig. 2. (a) Dependences of the EL conversion (blue sphere), EP yield (red sphere), acetaldehyde yield (orange sphere), ethanol yield (green sphere), other products (wine sphere), and carbon balance (gray sphere) on the reaction temperature over Cu/SiO_2-HP; (b) The EL conversion of ethyl lactate (blue column), EP selectivity (red column), and carbon balance (gray sphere) over various Cu-based catalysts during the dehydrogenation of EL to produce EP at 320 °C. The abbreviation of ethyl lactate, ethyl pyruvate, acetaldehyde, acetaldehyde, and ethanol were EL, EP, AcH, and EtOH, respectively. Reaction conditions: P_{EL} = 1.20 kPa, N_2 flow rate at 54.3 mL/min, 0.2 g of catalyst, and WHSV at 1.0 $g_{EL}{\cdot}g_{cat}^{-1}{\cdot}h^{-1}$.

increased from 21.0 % to 77.8 % in the temperature from 220 to 320 °C, but decreased from 77.8 % to 73.3 % in the temperature from 320 to 356 °C (Table S2). The side products that can be identified by GC-FID were acetaldehyde and ethanol. The ethanol yield was basically maintained at about 1 % in the temperature from 220 to 356 °C (Table S2). The acetaldehyde yield gradually ascended from 0.1 % to 5.6 % with increasing temperature from 220 to 356 °C (Table S2). The reduction in the EP yield observed at higher temperature may be related to the unstable nature of EP at high temperature, as confirmed by the TG-DSC analysis and FT-IR profile (Fig. S5). At 320 °C in the absence of O_2, Cu/SiO_2-HP exhibited the highest EP yield of 77.8 % (85.4 % EL conversion with 91.1 % EP selectivity) (Fig. 2a and Table S2), which was comparable to those observed for previously reported catalysts in the oxidative dehydrogenation of EL [2,5,6,10,14,15]. However, the EP selectivities over the oxidative dehydrogenation of EL were lower than 90.0 % (Table S3) [10,14,15]. The EP yield can be further improved by adjusting the WHSV from 1.0 to 0.5 $g_{EL}{\cdot}g_{cat}^{-1}{\cdot}h^{-1}$, where Cu/SiO_2-HP exhibited an 81.3 % EP yield with 88.6 % EL conversion at 303 °C (Figs. S6 and S7).

For comparison, we synthesized Cu/SiO_2-AE and Cu/SiO_2-IM *via* ammonia evaporation and impregnation methods (Figs. S8-S10 and Table S1). Cu/SiO_2-AE exhibited higher EL conversion (89.7 %) but lower EP selectivity (60.0 %) at 320 °C, where the major by-product of acetaldehyde was 16.4 %, which is much higher than the acetaldehyde yield of 2.3% over the Cu/SiO_2-HP (Fig. 2b and Table S4). Lower EP selectivity might be related to the relatively lower Cu^+ content in the Cu/SiO_2-AE (Figs. S11 and S12). The Cu/SiO_2-IM catalyst exhibited a much lower EP yield at 320 °C, giving EL conversion at 48.6 % and EP selectivity at 72.6 % (Fig. 2b). The low activity of the Cu/SiO_2-IM catalyst may be attributed to the low Cu dispersion (Figs. S13 and S14), as supported by the TEM image (Fig. S10) and measurement of N_2O titration (Table S1).

Furthermore, the acidic carriers supported Cu catalysts, *i.e.* Cu/Al_2O_3 and Cu/TiO_2 (Figs. S15-S17, and Table S5) also showed low selectivities (5.3 % and 30.1 %) at the reaction temperature of 320 °C, which exhibited the EP yield of 4.85 % and 6.20 % at the EL conversion of 91.6% and 20.6 %, respectively (Fig. 2b and Table S4). Their side products can be identified as acetaldehyde and ethanol. Ethanol was produced by the cleavage of ester bond under the action of acid sites from carriers [30,31]. Acetaldehyde was generated by the decomposition of EL *via* decarboxylation/decarbonylation pathways owing to the acid sites of carriers [29,32,33]. Others (probably coke) were 57.6 % and 9.66 % for Cu/Al_2O_3 and Cu/TiO_2. Formation of coke was most probably catalyzed by acid sites of carriers [28,29]. In addition, the Cu/TiO_2 has lower conversion than Cu/Al_2O_3 as a consequence of relatively lower Cu dispersion (Table S5). At the reaction temperature of 320 °C, the Cu catalysts that be supported onto the basic carriers, *i.e.* Cu/MgO showed low selectivity (5.8 %) at the EL conversion of 48.3 % (Fig. 2b and Table S4). The major side product was ethanol (the yield of 24.8 %) by reason that basic sites of carries could promote the cleavage of ester bond, and yield of others (oligomer/coke) was 16.5 % presumably due to the condensation of EL catalyzed by basic sites of carries [34,35].

3.2. *Structure-performance relationship*

To understand the excellent performance observed in the dehydrogenation of EL to EP over the Cu/SiO_2-HP catalyst, the Cu species in the catalysts were investigated by XANES and XPS techniques. As observed in Cu K-edge XANES spectra (Fig. 3a and b), the signal of Cu/SiO_2-HP was between those of Cu foil and Cu_2O (Fig. 3a and b), indicating that the average valence state of the Cu species in Cu/SiO_2-HP ranged from 0 to 1. After *in situ* reduction, Cu/SiO_2-HP exhibited a single $Cu2p_{3/2}$ peak at 933.6 eV on the Cu2p XPS spectrum (Fig. 3c), indicating the presence of Cu^0 and Cu^+ species on the catalyst surface. To determine the relative contents of Cu^0 and Cu^+ in Cu/SiO_2-HP (Fig. 3d), *in situ* Cu LMM spectroscopy was performed, and the resulting spectrum exhibited peaks at 569.6 and 573.1 eV, which can be associated with the surface Cu^0 and Cu^+ species [36–38]. After calculation by the peak area, the relative contents of Cu^0 and Cu^+ on the catalyst surface were estimated to be 27.8 % and 72.2 %, respectively.

The valence state of the surface Cu species was further investigated using *in situ* CO-adsorption FT-IR spectroscopy (Fig. 4a). Two bands were observed at 2112 and 2128 cm^{-1} in the FT-IR spectrum after the adsorption of CO at 30 °C, which were associated with the surface Cu^0 and Cu^+ species [39–42]. The relative contents of Cu^0 and Cu^+ were estimated to be 29.5 % and 70.5 %, respectively from the IR peak areas (Fig. 4a), which were in good agreement with those obtained from the XPS results (Fig. 3d). Furthermore, the CO saturation-adsorbed Cu/SiO_2-HP was exposed to a flow of EL and the band observed at 2128 cm^{-1} ($CO\text{-}Cu^+$) gradually decreased, whereas the band at 2112 cm^{-1} ($CO\text{-}Cu^0$) was unchanged. After being exposed to a flow of EL for 150 s, the relative contents of Cu^0 and Cu^+ on the catalyst surface were determined to be 51.2 % and 48.8 %, respectively (Fig. 4a). This

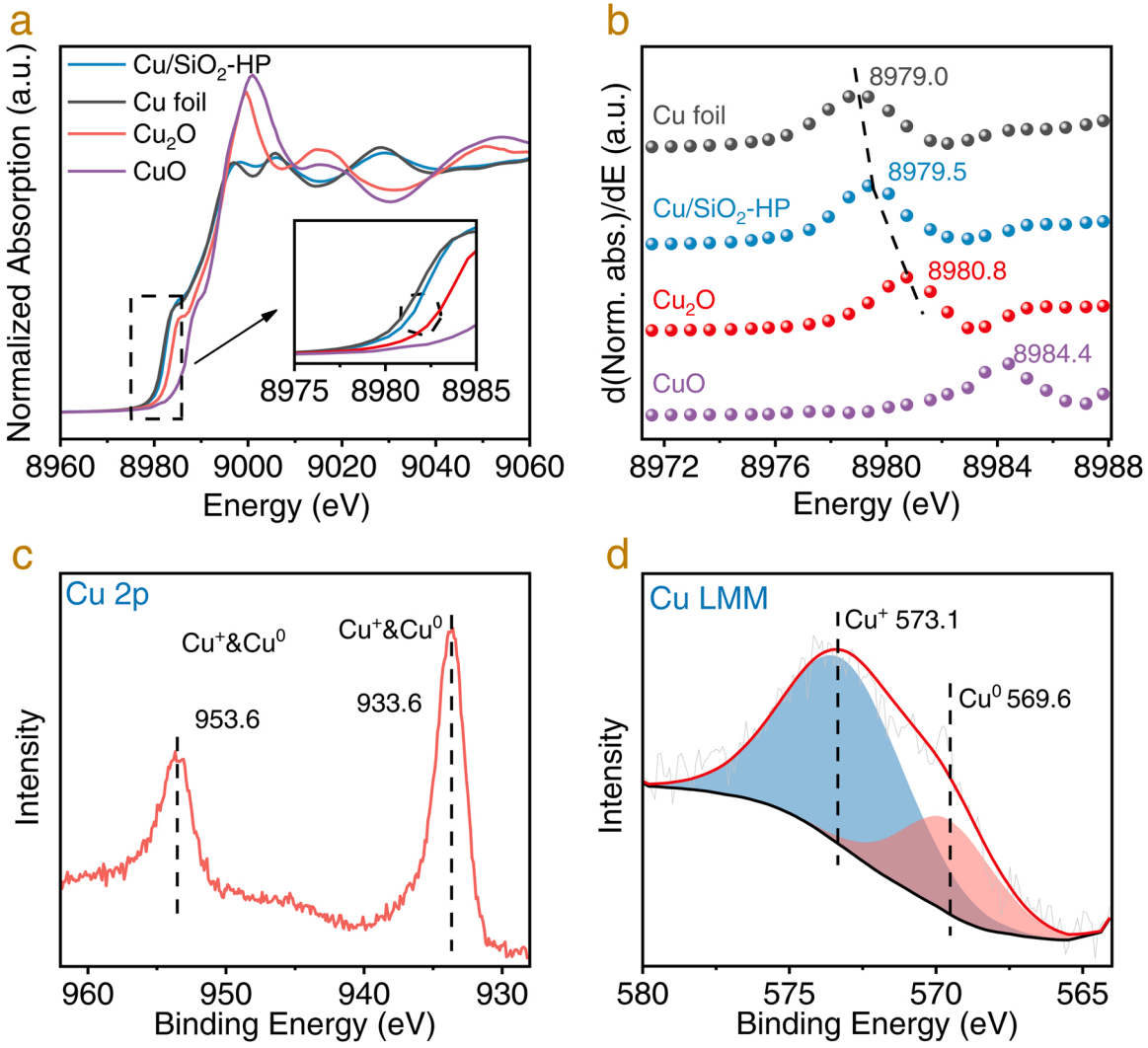

Fig. 3. (a) Normalized and (b) first derivative XANES spectra at the K-edge of Cu foil, Cu_2O, CuO, and Cu/SiO_2-HP; *In situ* (c) Cu2p and (d) Cu LMM spectra of the Cu/SiO_2-HP catalyst after reduction at 300 °C for 1 h.

phenomenon indicates the preferential interaction between EL molecule and the Cu^+ species [23]. When the CO and EL co-adsorbed Cu/SiO_2-HP was heated under a flow of helium gas, the intensity of the CO-adsorbed IR bands was significantly reduced upon increasing the temperature. When the temperature reached 100 °C, the peak corresponding to the CO-adsorbed IR band was shifted to 2128 cm^{-1} (CO-Cu^+), and the band related to (CO-Cu^0) observed at 2112 cm^{-1} almost disappeared (Fig. 4b). One possible explanation for these results may be that the interaction between EL with Cu^+ formed an intermediate, which can hinder the adsorption of CO on the Cu^0 sites [23].

The interaction of EL with the Cu^+ and Cu^0 species was also investigated by exposing EL to as-reduced Cu/SiO_2-HP catalyst (Fig. 5). After saturation adsorption of EL, a broad band at 3700–3200 cm^{-1} and several sharp bands in the range of 2920–2890 cm^{-1} appeared in the FT-IR spectra (Fig. 5), which should be associated with the ν_s(OH) and ν(CH) species in EL [43–46]. When the sample was heated at a rate of 10 °C/min under a flow of helium gas, the absorbance of the ν_s(OH) band decreased upon increasing the temperature, suggesting the conversion of the OH group in EL. When the temperature was increased to 100 °C, a band at 1645 cm^{-1} appeared in the FT-IR spectrum (Fig. 5), which can be attributed to a C═O bond coordinated to the catalytic site (Fig. S18) [47–50]. These results suggest the cleavage of the -OH group in EL to form a C═O group. At the same time, the H species can transfer to the nearby Cu^0 species, which may impede the adsorption of CO on the Cu^0 species, as shown in Fig. 4b and S18). A further increase of the temperature to 200 °C led to a decrease of the intensity of the band observed at 2908 cm^{-1} [ν(CH)] [5,6,45,51], suggesting that the α-C-H bond was cleaved to form EP (Fig. S18). Considering the preferential interaction of H species with the Cu^0 species, which was supported by hydrogen-deuterium exchange experiments (Fig. S19) [18,52,53], it is possible that cleavage of the α-C-H bond cleavage may occur on the Cu^0 species in Cu/SiO_2-HP.

After cleavage of the α-C-H bond, the as-formed H_2 and EP should be desorbed from the Cu/SiO_2-HP catalyst. Fig. 6 showed the temperature-programmed desorption (TPD) curves of H_2 and EP on Cu/SiO_2-HP. The H_2-TPD profile exhibited a peak at 118 °C for H_2 desorption, which was much lower than the reaction temperature. The EP-TPD profile exhibited two peaks at 149 and 289 °C for EL desorption. The ethyl pyruvate is a typical α-ketoester. The adsorption of α-ketoester on metals have been well investigated [54–56]. Fleming and co-workers have investigated the adsorption modes of methyl pyruvate (also as a α-ketoester) on Cu (111) in detail [56], showing that there were two chemical adsorption modes of ethyl pyruvate on Cu (111). At lower temperature, ethyl pyruvate is weakly adsorbed in Cu (111), which interacts with the surface through the lone pair electrons of the oxygen atoms of the C═O groups, adopting a η_1 configuration (Fig. S20). At higher temperature, its keto-carbonyl bonded to the surface in a η_2 configuration. On the EP-TPD profile, two peaks at 149 and 289 °C correspond to two modes

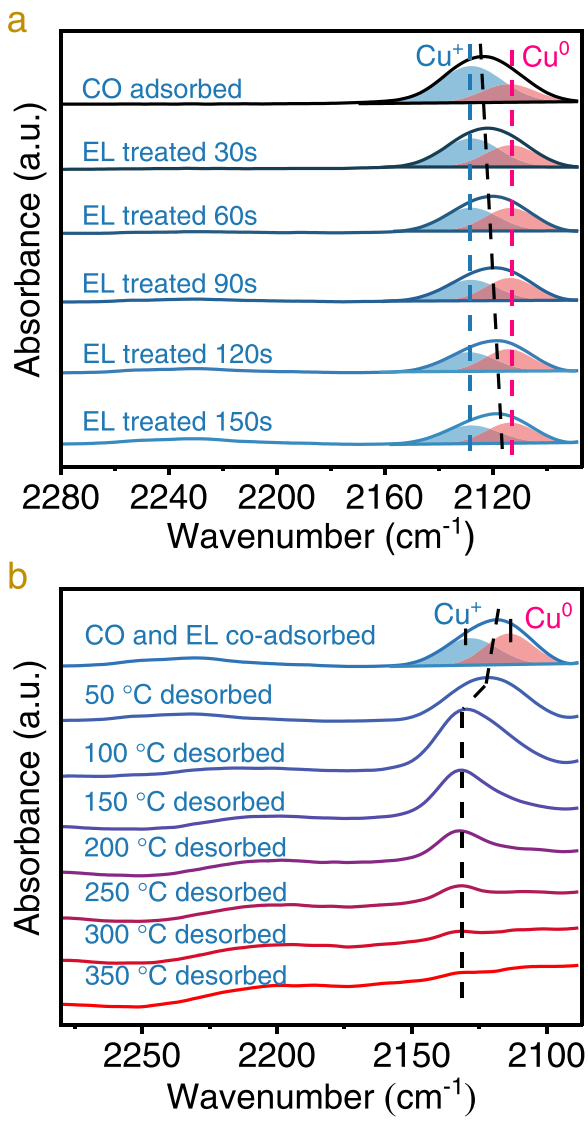

Fig. 4. *In situ* FT-IR spectra of the Cu/SiO_2-HP after (a) the adsorption of CO and treatment with EL at 30 °C and (b) sequential temperature-programmed treatment at a heating rate of 10 °C/min.

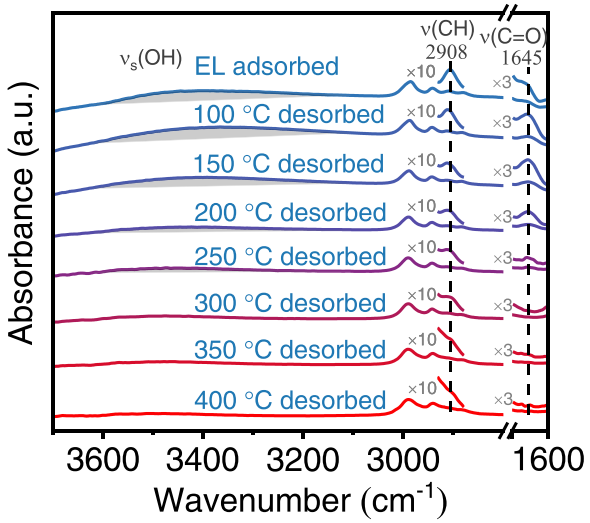

Fig. 5. *In situ* FT-IR spectra of the Cu/SiO_2-HP after the adsorption of EL at 30 °C and sequential temperature-programmed treatment at a heating rate of 10 °C/min.

mentioned above, respectively. Notably, the temperatures for H_2 and EL desorption were obviously lower than the reaction temperature, indicating that the desorption of the catalytic products was relatively easy. Therefore, the rate-determining step in the dehydrogenation of EL to EP was related to the cleavage of the -OH or α-C-H bonds in EL.

It has been reported that H/D kinetic isotope effects (KIE) are sensitive to the reaction rate [57], but it is difficult to obtain deuterium-substituted EL. Due to the similar reaction pathways for the dehydrogenation of ethanol and ethyl lactate [23], we studied the KIE of deuterium-substituted ethanol during the dehydrogenation reactions, as shown in Fig. 7. The results showed that Cu/SiO_2-HP exhibited TOF values of 2.74, 1.72, and 0.58 mmol·g_{cat}^{-1}·min^{-1} when ethanol-d_0, 1-D-ethanol, and ethanol-d_6 were employed as the substrates, respectively (Fig. 7). The KIE values for the pair of ethanol-d_0 and 1-D-ethanol ($KIE_{0D/1D}$) was 1.59 (Fig. 7), which was much lower than that (4.72) for the pair of ethanol-d_0 and ethanol-d_6 ($KIE_{0D/6D}$). Considering that ethanol dehydrogenation proceeds *via* the sequential cleavage of the O-H and C-H bonds, the C-H bond cleavage reaction should be the rate-determining step. As ethanol dehydrogenation is the sister reaction to EL dehydrogenation, it is reasonable to deduce that C-H bond cleavage could also be the rate-determining step in the EL dehydrogenation reaction performed over Cu/SiO_2-HP.

Based on the aforementioned results, it can be concluded that the dehydrogenation of EL was catalyzed by the synergism of Cu^0/Cu^+, as proposed by the reaction mechanism shown in Fig. S18. Therefore, the catalytic performance of Cu/SiO_2-HP should be related to the Cu^0/Cu^+ interface [37,58]. To verify this hypothesis, Cu/SiO_2-HP catalysts with different Cu^0/Cu^+ interface lengths were synthesized by adjusting the Cu loading in the catalysts (Fig. S21). Interestingly, the TOF values of these Cu/SiO_2-HP catalysts increased almost linearly upon increasing the number of Cu^0/Cu^+ interfaces (Fig. 8), confirming the synergism of Cu^0/Cu^+ in Cu/SiO_2-HP for dehydrogenation of EL to produce EP.

3.3. DFT simulations

Theoretical calculations were performed to further understand the dehydrogenation mechanism of Cu/SiO_2-HP (Fig. 9). The -OH group in EL was initially absorbed on the positively charged Cu atoms (Cu^+) in the Cu/SiO_2-HP (Fig. S22a and S22b), releasing energy of 0.29 eV (Fig. 9, S22c, and S22d). The reaction started from the cleavage of the O-H bond in the -OH group *via* the synergy of the Cu^0/Cu^+ interface, exhibiting an activation barrier of 0.86 eV (step A to B in Fig. 9). The as-formed H atoms were bonded to the Cu^0 atoms on the catalyst (Fig. 9, S22g, and S22h). These results were in accordance with the *in situ* FT-IR spectra (Figs. 4 and 5). Then, the catalyst proceeded to cleave the C-H bond in the intermediate *via* the synergy of the positively charged and other metallic Cu atoms, exhibiting an activation barrier of 1.08 eV (step B to C in Fig. 9), which was higher than that of the O-H cleavage step (0.86 eV). This phenomenon indicates that C-H bond cleavage is the rate-determining step for the dehydrogenation of EL to EP, which was in good agreement with the *in situ* FT-IR spectra (Figs. 4 and 5) and the KIE experiments (Fig. 7). The desorption of H_2 has been reported to be difficult for some Cu^+-containing catalysts [23]. Therefore, it is valuable to calculate the desorption of H_2 from Cu/SiO_2-HP. The desorption of H_2 proceeded *via* the association of the H atoms to form gaseous H_2 on an adjacent Cu^0 atom, exhibiting an activation barrier of 0.41 eV (step D to E in Fig. 9). The low activation barrier indicates that the desorption of H_2 proceeded easily on Cu/SiO_2-HP, which was in accordance with the results obtained from the H_2-TPD curve (Fig. 6).

3.4. Recyclable tests

The recyclable tests for Cu/SiO_2-HP was also studied at 275 °C with

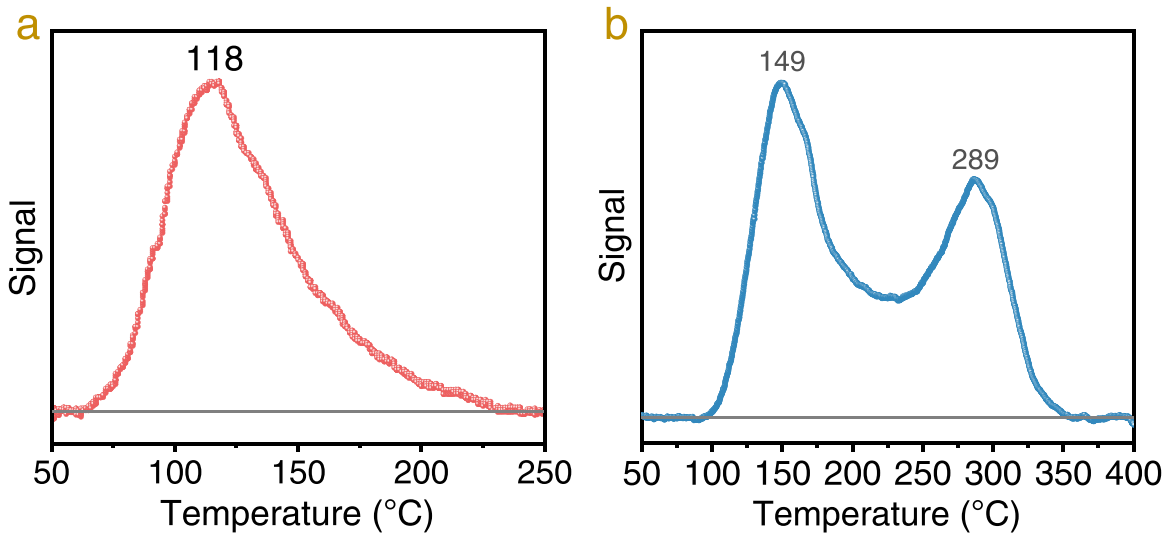

Fig. 6. Temperature-programmed desorption of (a) H_2 and (b) EP over Cu/SiO_2-HP.

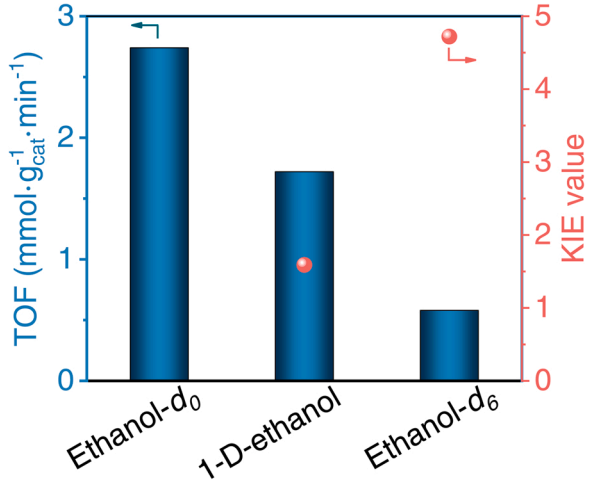

Fig. 7. H/D Kinetic isotope effect for ethanol dehydration (separate substrates) over Cu/SiO_2-HP. Reaction conditions: $P_{Ethanol}$ = 0.66 kPa, P_{N2} = 100.67 kPa, 0.006–0.014 g of catalyst, GHSV at 235714–550000 mL·g$^{-1}_{cat}$·h^{-1}, and 210 °C.

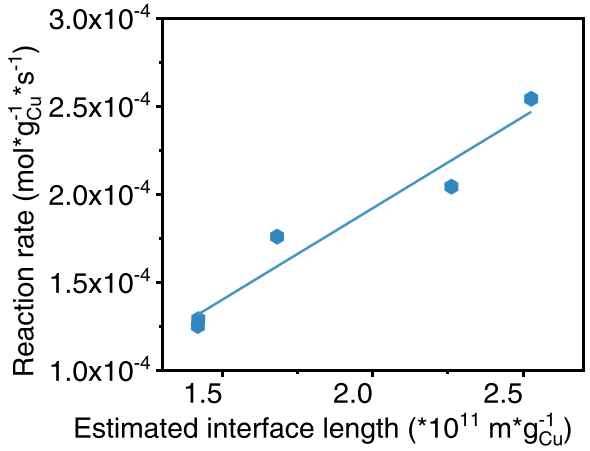

Fig. 8. Reaction rate as a function of the Cu^0-Cu^+ interface length over Cu/SiO_2-HP with different Cu loadings.

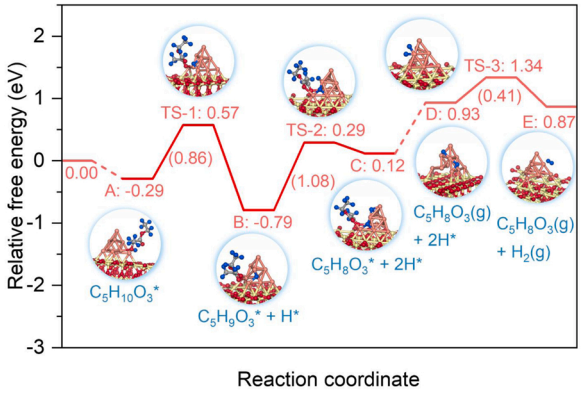

Fig. 9. Energy profile for EL dehydrogenation on Cu/SiO_2-HP.

WHSV at 0.5 g_{EL}·g$^{-1}_{cat}$·h^{-1}. As shown in Fig. S23, the EL conversion and EP yield slowly decreased with the reaction time. After reaction for 7 h, the EL conversion decreased from 89.1 % to 83.4 %, and EP yield decreased from 79.5 % to 76.7 %, respectively. Calcination at 400 °C under a flow of O_2 gas, followed by sequential reduction at 300 °C under a flow of H_2 restored the catalytic performance. The regenerated catalyst exhibited an EP yield of 79.8 % (2nd circle in Fig. S23), which were similar to those of the fresh catalyst. Even after regeneration for 3 times, the regenerated catalyst exhibited an EP yield at 78.4 %, which were slightly lower than that (79.5 %) of the fresh catalyst (3rd circle in Fig. S23).

The deactivation of Cu/SiO_2-HP in the direct dehydrogenation of EL to EP was also investigated. The used Cu/SiO_2-HP catalyst exhibited larger Cu nanoparticles than the fresh one (Fig. S24). Besides metal sintering, coke formation is also one of the major reasons for the deactivation of heterogeneous catalysts. Because the Cu/SiO_2-HP catalyst exhibited different deactivation rate after catalyzing reaction for 1–6 h and 6–23 h, we have performed thermogravimetric analysis-differential scanning calorimetry (TG-DSC) curves of the Cu/SiO_2-HP catalyst used for 6 h and 23 h (designated as Cu/SiO_2-HP-u6h and Cu/SiO_2-HP-u23h) to study the coke formation. As shown in Fig. S25a, the Cu/SiO_2-HP-u6h exhibited three stages of mass loss in the temperature ranges of room temperature (RT)– 130, 130–270, and 270–550 °C on the TG curve. Based on the DSC curves, the ranges at RT-130 and 130–270 °C were endothermic and the range at 270–550 °C was exothermic (Fig. S25a), indicating that the mass loss at RT-270 °C was caused by the evaporation of adsorbed species (ethyl lactate and reaction products) and the mass

loss at 270–550 °C was caused by calcination of coke species. Based on the TG curves, the coke amount on the Cu/SiO_2-HP-u6h was ~2.8 *wt*% (Fig. S25a). Therefore, it can be concluded that the deactivation at 0–6 h was mainly resulted from the coke formation.

The Cu/SiO_2-HP-u23h exhibited similar trend for the mass loss (Fig. S25b). The mass loss at RT-270 °C was also caused by the evaporation of adsorbed species. Interestingly, the Cu/SiO_2-HP-u23h exhibited a 0.7 *wt*% mass increase at 270–300 °C (Fig. S25b), which was not obvious on the TG curve of the Cu/SiO_2-HP-u6h (Fig. S25a). Considering that the used Cu/SiO_2-HP catalyst only contained C, O, H, Cu, Si, and O species, it was reasonable that the mass increase at 270–300 °C was related to the oxidation of Cu^0 species. To prove this hypothesis, we have performed XPS analysis of the Cu/SiO_2-HP-u23h. As shown in Fig. S26a, the Cu/SiO_2-HP-u23h exhibited a single $Cu2p_{3/2}$ peak at 932.6 eV on the Cu2p XPS spectrum, indicating the presence of Cu^0 and Cu^+ species on the catalyst surface. To determine the relative contents of Cu^0 and Cu^+ in Cu/SiO_2-HP, *in situ* Cu LMM spectroscopy was performed (Fig. S26b), and the resulting spectrum exhibited peaks at 569.6 and 573.1 eV, which can be associated with the surface Cu^0 and Cu^+ species [36–38]. After calculation by the peak area, the relative contents of Cu^0 on the Cu/SiO_2-HP-u23h catalyst were estimated to be 50.1 %, which was much higher than that (27.8 %) on the fresh catalyst. This phenomenon suggests that the copper species could be reduced to Cu^0 during the reaction time at 6–23 h (Fig. S27). Considering that the Cu^0/Cu^+ interfaces were the catalytic active sites, the reduction of copper species should be one of major reasons for the deactivation.

Furthermore, the coke amount on the Cu/SiO_2-HP-u23h was estimated at ~3.1 *wt*% (Fig. S25b). Although this value was only a little higher than that (~2.8 *wt*%) on the Cu/SiO_2-HP catalyst used for 6 h (Fig. S25a), the component of the coke species on the Cu/SiO_2-HP-u6h and Cu/SiO_2-HP-u23h might be different. We performed FT-IR spectra of the used Cu/SiO_2-HP catalyst to study the coke species. As shown in Fig. S28, the Cu/SiO_2-HP-u6h showed bands at 3600–3200, 2987, and 1732 cm^{-1}, which were associated with the O-H, C-H, and C═O bonds [5,6]. This phenomenon implies that the coke species on the Cu/SiO_2-HP-u6h are derived from the oligomerization of ethyl lactate and ethyl pyruvate species. In contrast, more bands at 3200–2800 and 1800–1550 cm^{-1} appeared on the FT-IR spectrum of the Cu/SiO_2-HP-u23h, which are associated with the C-H and C-C bonds on aromatic compounds [29,59]. This phenomenon indicates that the coke species formed during the reaction time at 6–23 h have been aromatized. It is well known that the aromatic compounds-containing cokes were more negative than the oligomers for the deactivation of lactates conversion reactions [29,60], a deep coke formation (aromatic compounds) should also be a critical reason for the deactivation of the Cu/SiO_2-HP catalyst in the reaction time at 6–23 h.

Based on the aforementioned results, it can be concluded that the deactivation at 0–6 h was mainly caused by coke formation, while the deactivation at 6–23 h was caused by both the coke formation and copper species reduction.

4. Conclusion

In conclusion, we have synthesized a Cu/SiO_2-HP catalyst with highly dispersed Cu nanoparticles using a hydrolysis–precipitation method for the direct dehydrogenation of EL into EP, which exhibited an 85.4 % EL conversion with 91.1 % EP selectivity at 320 °C. Characterizations, kinetic studies, and theoretical calculations have demonstrated that the dehydrogenation of EL proceeded on the Cu^0/Cu^+ interface, which synergistically activated the O−H and C−H bonds in the adsorbed EL, respectively. The H/D kinetic isotope effect for model reaction confirmed that C−H bond activation is the key step in the dehydrogenation reaction. The highly dispersed Cu nanoparticles result in the formation of abundant Cu^0/Cu^+ interfaces, which are essential for the excellent catalytic performance of Cu/SiO_2-HP. Due to the coke formation and copper species reduction, the reaction rate of Cu/SiO_2-HP was reduced gradually. Therefore, the catalytic stability should be improved in the future, which was under investigation in our laboratory. This study is beneficial for understanding the structure-catalytic performance of the dehydrogenation of EL to form EP. This study offers a new approach for the conversion of EL to EP in the future.

CRediT authorship contribution statement

Shiyao Lu: Conceptualization, Methodology, Investigation. **Jian Zhang:** Conceptualization, Methodology, Writing – original draft. **Hao Meng:** Methodology, Investigation. **Xiaoyuan Qin:** Methodology, Investigation. **Jianbin Huang:** Methodology, Investigation. **Yehao Liang:** Methodology, Investigation. **Feng-Shou Xiao:** Supervision, Writing – review & editing.

Declaration of Competing Interest

The authors declare that they have no known competing financial interests or personal relationships that could have appeared to influence the work reported in this paper.

Data availability

Data will be made available on request.

Acknowledgements

This work is supported by the National Key Research and Development Program of China (2018YFB0604801), the National Natural Science Foundation of China (22002007), and the Fundamental Research Funds for the Central Universities (XK2022-12). The authors are thankful for the support of the BSRF (Beijing Synchrotron Radiation Facility) during the XAFS measurements at the beamline of 1W1B.

Appendix A. Supporting information

Supplementary data associated with this article can be found in the online version at doi:10.1016/j.apcatb.2022.122329.

References

[1] C. Mondelli, G. Gozaydin, N. Yan, J. Perez-Ramirez, Biomass valorisation over metal-based solid catalysts from nanoparticles to single atoms, Chem.. Soc. Rev. 49 (2020) 3764–3782.
[2] J. Pang, J. Sun, M. Zheng, H. Li, Y. Wang, T. Zhang, Transition metal carbide catalysts for biomass conversion: a review, Appl. Catal. B-Environ. 254 (2019) 510–522.
[3] T. Lu, J. Zou, Y. Zhan, X. Yang, Y. Wen, X. Wang, L. Zhou, J. Xu, Highly efficient oxidation of ethyl lactate to ethyl pyruvate catalyzed by TS-1 under mild conditions, ACS Catal. 8 (2018) 1287–1296.
[4] W. Zhang, B. Ensing, G. Rothenberg, N.R. Shiju, Designing effective solid catalysts for biomass conversion: aerobic oxidation of ethyl lactate to ethyl pyruvate, Green Chem. 20 (2018) 1866–1873.
[5] W. Zhang, G. Innocenti, M. Ferbinteanu, E.V. Ramos-Fernandez, A. Sepulveda-Escribano, H.H. Wu, F. Cavani, G. Rothenberg, N.R. Shiju, Understanding the oxidative dehydrogenation of ethyl lactate to ethyl pyruvate over vanadia/titania, Catal. Sci. Technol. 8 (2018) 3737–3747.
[6] W. Zhang, G. Innocenti, P. Oulego, V. Gitis, H. Wu, B. Ensing, F. Cavani, G. Rothenberg, N.R. Shiju, Highly selective oxidation of ethyl lactate to ethyl pyruvate catalyzed by mesoporous vanadia-titania, ACS Catal. 8 (2018) 2365–2374.
[7] D.S. Doke, S.B. Khomane, S.L. Pandhare, M.K. Dongare, F. Dumeignil, S. B. Umbarkar, Vanadium-based highly active and selective catalysts for oxidative dehydrogenation of ethyl lactate to ethyl pyruvate, Appl. Catal. A Gen. 587 (2019), 117246.
[8] W. Zhang, P. Oulego, T.K. Slot, G. Rothenberg, N.R. Shiju, Selective aerobic oxidation of lactate to pyruvate catalyzed by vanadium-nitrogen-doped carbon nanosheets, ChemCatChem 11 (2019) 3381–3387.
[9] Z. Zhang, S. Ishikawa, Q. Zhu, T. Murayama, M. Sadakane, M. Hara, W. Ueda, Redox-active zeolitic transition metal oxides based on epsilon-keggin units for selective oxidation, Inorg. Chem. 58 (2019) 6283–6293.

[10] M. Huchede, D. Morvan, V. Bellière-Baca, J.M.M. Millet, Screening of catalysts for the oxidative dehydrogenation of ethyl lactate to ethyl pyruvate, and optimization of the best catalysts, Appl. Catal. A Gen. 601 (2020), 117619.

[11] L. Tao, X. Bi, L. Zhang, G. Chen, P. Zhao, J.-L. Yang, X. Meng, Na-doped OMS-2-catalzyed highly selective aerobic oxidation of ethyl lactate to ethyl pyruvate under mild conditions, Appl. Catal. A Gen. 605 (2020), 117813.

[12] G. Wang, P. Wang, X. Zhang, Q.H. Wei, S. Wu, Z. Xie, Nucleobase derived boron and nitrogen co-doped carbon nanosheets as efficient catalysts for selective oxidation and reduction reactions, Nanoscale 12 (2020) 7797–7803.

[13] J. Wu, W. Hua, Y. Yue, Z. Gao, Efficient aerobic oxidation of ethyl lactate to ethyl pyruvate over V_2O_5/g-C_3N_4 catalysts, ACS Omega 5 (2020) 16200–16207.

[14] W. Zhang, P. Oulego, S.K. Sharma, X.-L. Yang, L.-J. Li, G. Rothenberg, N.R. Shiju, Self-exfoliated synthesis of transition metal phosphate nanolayers for selective aerobic oxidation of ethyl lactate to ethyl pyruvate, ACS Catal. 10 (2020) 3958–3967.

[15] M. Huchede, D. Morvan, R. Vera, V. Bellière-Baca, J.M.M. Millet, Oxidative dehydrogenation of ethyl lactate to ethyl pyruvate over vanadium and iron antimonates catalysts, Appl. Catal. A Gen. 617 (2021), 118016.

[16] B. Hočevar, M. Grilc, M. Huš, B. Likozar, Mechanism, Ab initio calculations and microkinetics of hydrogenation,hydrodeoxygenation, double bond migration and cis–transisomerisation during hydrotreatment of C6 secondary alcohol speciesand ketones, Appl. Catal. B Environ. 218 (2017) 147–162.

[17] R. Šivec, M. Grilc, M. Huš, B. Likozar, Multiscale modeling of (hemi)cellulose hydrolysis and cascade hydrotreatment of 5–hydroxymethylfurfural, furfural, and levulinic acid, Ind. Eng. Chem. Res. 58 (2019) 16018–16032.

[18] B. Hočevara, M. Grilca, M. Huš, B. Likozar, Mechanism, ab initio calculations and microkinetics of straight-chain alcohol, ether, ester, aldehyde and carboxylic acid hydrodeoxygenation over Ni-Mo catalyst, Chem. Eng. J. 359 (2019) 1339–1351.

[19] R. Šivec, M. Huš, B. Likozar, M. Grilc, Furfural hydrogenation over Cu, Ni, Pd, Pt, Re, Rh and Ru catalysts: ab initio modelling of adsorption, desorption and reaction micro-kinetics, Chem. Eng. J. 436 (2022), 135070.

[20] A. Kojčinović, Z. Kovačič, M. Huš, B. Likozar, M. Grilc, Furfural hydrogenation, hydrodeoxygenation and etherification over MoO2 and MoO3: A combined experimental and theoretical study, Appl. Surf. Sci. 543 (2021), 148836.

[21] X. Xiao, C. Zheng, M. Lu, L. Zhang, F. Liu, X. Zuo, J. Nan, Deficient $Bi_{24}O_{31}Br_{10}$ as a highly efficient photocatalyst for selective oxidation of benzyl alcohol into benzaldehyde under blue LED irradiation, Appl. Catal. B Environ. 228 (2018) 142–151.

[22] S. Kondaveeti, G.D. Park, R. Shanmugam, R. Pagolu, S.K.S. Patel, A. Bisht, D. R. Kim, Y.C. Kang, J.K. Lee, Investigating the role of metals loaded on nitrogen-doped carbon-nanotube electrodes in electroenzymatic alcohol dehydrogenation, Appl. Catal. B Environ. 307 (2022), 121195.

[23] J. Pang, M. Zheng, C. Wang, X. Yang, H. Liu, X. Liu, J. Sun, Y. Wang, T. Zhang, Hierarchical echinus-like Cu-MFI catalysts for ethanol dehydrogenation, ACS Catal. 10 (2020) 13624–13629.

[24] M. Guo, P. Ma, J. Wang, H. Xu, K. Zheng, D. Cheng, Y. Liu, G. Guo, H. Dai, E. Duan, J. Deng, Synergy in Au-CuO Janus structure for catalytic isopropanol oxidative dehydrogenation to acetone, Angew. Chem., Int. Ed. 61 (2022), e202203827.

[25] G. Giannakakis, P. Kress, K. Duanmu, H.T. Ngan, G. Yan, A.S. Hoffman, Z. Qi, A. Trimpalis, L. Annamalai, M. Ouyang, J. Liu, N. Eagan, J. Biener, D. Sokaras, M. Flytzani-Stephanopoulos, S.R. Bare, P. Sautet, E.C.H. Sykes, Mechanistic and electronic insights into a working NiAu single-atom alloy ethanol dehydrogenation catalyst, J. Am. Chem. Soc. 143 (2021) 21567–21579.

[26] T. Wang, J. Sha, M. Sabbe, P. Sautet, M. Pera-Titus, C. Michel, Identification of active catalysts for the acceptorless dehydrogenation of alcohols to carbonyls, Nat. Commun. 12 (2021) 5100.

[27] Y. Zhao, S. Li, Y. Wang, B. Shan, J. Zhang, S. Wang, X. Ma, Efficient tuning of surface copper species of Cu/SiO_2 catalyst for hydrogenation of dimethyl oxalate to ethylene glycol, Chem. Eng. J. 313 (2017) 759–768.

[28] B.M. Murphy, M.P. Letterio, B. Xu, Selectivity control in the catalytic dehydration of methyl lactate: the effect of pyridine, ACS Catal. 6 (2016) 5117–5131.

[29] E.V. Makshina, J. Canadell, J. van Krieken, B.F. Sels, Potassium-modified ZSM-5 catalysts for methyl acrylate formation from methyl lactate: the impact of the intrinsic properties on their stability and selectivity, ACS Sustain. Chem. Eng. 10 (2022) 6196–6204.

[30] J.W. Jeong, C.-I. Ahn, D.H. Lee, S.H. Um, J.W. Bae, Effects of Cu–ZnO content on reaction rate for direct synthesis of DME from syngas with bifunctional Cu–ZnO/γ-Al_2O_3 catalyst, Catal. Lett. 143 (2013) 666–672.

[31] P. Sudarsanam, H. Li, T.V. Sagar, TiO_2-based water-tolerant acid catalysis for biomass-based fuels and chemicals, ACS Catal. 10 (2020) 9555–9584.

[32] S. Furukawa, M. Ieda, K.-i Shimizu, Heterogeneous additive-free hydroboration of alkenes using Cu–Ni/Al_2O_3: concerted catalysis assisted by acid–base properties and alloying effects, ACS Catal. 9 (2019) 5096–5103.

[33] L. Lv, S. Wang, Y. Ding, L. Zhang, Y. Gao, S. Wang, Mechanistic insights into the contribution of Lewis acidity to brominated VOCs combustion over titanium oxide supported Ru catalyst, Chemosphere 263 (2021), 128112.

[34] H. Li, X. Zheng, H. Zhang, X. Li, J. Long, Selective cleavage of ester linkages in lignin catalyzed by La-doped Ni/MgO, ACS Sustain. Chem. Eng. 8 (2020) 15685–15695.

[35] K.K. Ramasamy, M. Gray, H. Job, D. Santosa, X.S. Li, A. Devaraj, A. Karkamkar, Y. Wang, Role of calcination temperature on the hydrotalcite derived MgO–Al_2O_3 in converting ethanol to butanol, Top. Catal. 59 (2016) 46–54.

[36] Y. Wang, H. Zhao, M. Li, J. Fan, G. Zhao, Magnetic ordered mesoporous copper ferrite as a heterogeneous Fenton catalyst for the degradation of imidacloprid, Appl. Catal. B Environ. 147 (2014) 534–545.

[37] A. Li, D. Yao, Y. Yang, W. Yang, Z. Li, J. Lv, S. Huang, Y. Wang, X. Ma, Active Cu^0-$Cu^{\sigma+}$ sites for the hydrogenation of carbon-oxygen bonds over Cu/CeO_2 catalysts, ACS Catal. 12 (2022) 1315–1325.

[38] C. Xu, G. Chen, Y. Zhao, P. Liu, X. Duan, L. Gu, G. Fu, Y. Yuan, N. Zheng, Interfacing with silica boosts the catalysis of copper, Nat. Commun. 9 (2018) 3367.

[39] A. Wolfbeisser, G. Kovács, S.M. Kozlov, K. Föttinger, J. Bernardi, B. Klötzer, K. M. Neyman, G. Rupprechter, Surface composition changes of CuNi-ZrO_2 during methane decomposition: an operando NAP-XPS and density functional study, Catal. Today 283 (2017) 134–143.

[40] H. Xie, D. Yi, L. Shi, X. Meng, High performance of CuY zeolite for catalyzing acetylene carbonylation and the effect of copper valence states on catalyst, Chem. Eng. J. 313 (2017) 663–670.

[41] M. Morán-Pineda, S. Castillo, M. Asomoza, R. Gómez, Copper oxide on Cu/Al_2O_3-TiO_2 catalysts TG, FTIR-CO absorption and catalytic activity in the NO reduction by CO, J. Therm. Anal. Calorim. 73 (2003) 341–346.

[42] C.Y. Wang, P. Ray, Q. Gong, Y. Zhao, J. Li, A.D. Lueking, Influence of gas packing and orientation on FTIR activity for CO chemisorption to the Cu paddlewheel, Phys. Chem. Chem. Phys. 17 (2015) 26766–26776.

[43] G. Cammas, M. Morssli, E. Fabregue, L. Bardet, Vibrational spectra of lactic acid and lactates, J. Raman Spectrosc. 22 (1991) 409–413.

[44] B. Wen, Y. Li, C. Chen, W. Ma, J. Zhao, An unexplored O_2-involved pathway for the decarboxylation of saturated carboxylic acids by TiO_2 photocatalysis: an isotopic probe study, Chem. Eur. J. 16 (2010) 11859–11866.

[45] Y. Chen, Y. Lin, Z. Peng, J. Lin, Transmission FT-IR Study on the adsorption and reactions of lactic acid and poly (lactic acid) on TiO_2, J. Phys. Chem. C 114 (2010) 17720–17727.

[46] S. Ligot, M. Guillaume, P. Raynaud, D. Thiry, V. Lemaur, T. Silva, N. Britun, J. Cornil, P. Dubois, R. Snyders, Experimental and theoretical study of the plasma chemistry of ethyl lactate plasma polymerization discharges, Plasma Process. Polym. 12 (2015) 405–415.

[47] T.V. Andrushkevich, G. Ya, Popova, Mechanism of heterogeneous oxidation of acrolein to acrylic acid, Russ. Chem. Rev. 60 (1991) 1023–1034.

[48] V.V. Kaichev, Y.A. Chesalov, A.A. Saraev, A.Y. Klyushin, A. Knop-Gericke, T. V. Andrushkevich, V.I. Bukhtiyarov, Redox mechanism for selective oxidation of ethanol over monolayer V_2O_5/TiO_2 catalysts, J. Catal. 338 (2016) 82–93.

[49] A. Chieregato, C. Bandinelli, P. Concepción, M.D. Soriano, F. Puzzo, F. Basile, F. Cavani, J.M. Nieto, Structure-reactivity correlations in vanadium-containing catalysts for one-pot glycerol oxidehydration to acrylic acid, ChemSusChem 10 (2017) 234–244.

[50] X. Zhang, G. Cui, H. Feng, L. Chen, H. Wang, B. Wang, X. Zhang, L. Zheng, S. Hong, M. Wei, Platinum-copper single atom alloy catalysts with high performance towards glycerol hydrogenolysis, Nat. Commun. 10 (2019) 5812.

[51] K. Hanai, A. Kuwae, K.-K. Kunimoto, S.-I. Kitoh, Vibrational spectra and normal coordinate analysis of lithium pyruvate monohydrate and its isotopic compounds, Eur. J. Chem. 5 (2014) 305–310.

[52] M.E. Witzke, P.J. Dietrich, M.Y. Ibrahim, K. Al-Bardan, M.D. Triezenberg, D. W. Flaherty, Spectroscopic evidence for origins of size and support effects on selectivity of Cu nanoparticle dehydrogenation catalysts, Chem. Commun. 53 (2017) 597–600.

[53] E. Yuan, P. Ni, W. Zhuang, R. Jian, P. Jian, Synergic catalysis by a CuO-like phase and Cu^0 for anaerobic dehydrogenation of 2,3-butanediol, J. Catal. 382 (2020) 256–268.

[54] M. Castonguay, J.-R. Roy, A. Rochefort, P.H. McBreen, Orientation and conformation of methyl pyruvate on Ni(111), J. Am. Chem. Soc. 122 (2000) 518–524.

[55] J.M. Bonello, F.J. Williams, A.K. Santra, R.M. Lambert, Fundamental aspects of enantioselective heterogeneous catalysis: the surface chemistry of methyl pyruvate on Pt{111}, J. Phys. Chem. B 104 (2000) 9696–9703.

[56] C. Fleming, J. Johnston, M. Kadodwala, An investigation of the surface chemistry of methyl pyruvate on Cu(1 1 1), Surf. Sci. 601 (2007) 5485–5491.

[57] F. Chen, M. Shetty, M. Wang, H. Shi, Y. Liu, D.M. Camaioni, O.Y. Gutiérrez, J. A. Lercher, Differences in mechanism and rate of zeolite-catalyzed cyclohexanol dehydration in apolar and aqueous phase, ACS Catal. 11 (2021) 2879–2888.

[58] J. Zhu, Y. Su, J. Chai, V. Muravev, N. Kosinov, E.J.M. Hensen, Mechanism and nature of active sites for methanol synthesis from CO/CO_2 on Cu/CeO_2, ACS Catal. 10 (2020) 11532–11544.

[59] H.-Z. Wang, L.-L. Sun, Z.-J. Sui, Y.-A. Zhu, G.-H. Ye, D. Chen, X.-G. Zhou, W.-K. Yuan, Coke formation on Pt–Sn/Al_2O_3 catalyst for propane dehydrogenation, Ind. Eng. Chem. Res. 57 (2018) 8647–8654.

[60] K. Qian, D.C. Tomczak, E.F. Rakiewicz, R.H. Harding, G. Yaluris, W. Cheng, X. Zhao, A.W. Peters, Coke formation in the fluid catalytic cracking process by combined analytical techniques, Energy Fuel. 11 (1997) 596–601.